

DESY-07-039
March 2007

Diffractive Photoproduction of $D^{*\pm}(2010)$ at HERA

ZEUS Collaboration

Abstract

Diffractive photoproduction of $D^{*\pm}(2010)$ mesons was measured with the ZEUS detector at the ep collider HERA, using an integrated luminosity of 78.6 pb^{-1} . The D^* mesons were reconstructed in the kinematic range: transverse momentum $p_T(D^*) > 1.9 \text{ GeV}$ and pseudorapidity $|\eta(D^*)| < 1.6$, using the decay $D^{*+} \rightarrow D^0 \pi_s^+$ followed by $D^0 \rightarrow K^- \pi^+$ (+c.c.). Diffractive events were identified by a large gap in pseudorapidity between the produced hadronic state and the outgoing proton. Cross sections are reported for photon-proton centre-of-mass energies in the range $130 < W < 300 \text{ GeV}$ and for photon virtualities $Q^2 < 1 \text{ GeV}^2$, in two ranges of the Pomeron fractional momentum $x_{IP} < 0.035$ and $x_{IP} < 0.01$. The relative contribution of diffractive events to the inclusive $D^{*\pm}(2010)$ photoproduction cross section is about 6%. The data are in agreement with perturbative QCD calculations based on various parameterisations of diffractive parton distribution functions. The results are consistent with diffractive QCD factorisation.

The ZEUS Collaboration

S. Chekanov¹, M. Derrick, S. Magill, B. Musgrave, D. Nicholass², J. Repond, R. Yoshida
Argonne National Laboratory, Argonne, Illinois 60439-4815, USA ⁿ

M.C.K. Mattingly

Andrews University, Berrien Springs, Michigan 49104-0380, USA

M. Jechow, N. Pavel [†], A.G. Yagües Molina

Institut für Physik der Humboldt-Universität zu Berlin, Berlin, Germany

S. Antonelli, P. Antonioli, G. Bari, M. Basile, L. Bellagamba, M. Bindi, D. Boscherini,
A. Bruni, G. Bruni, L. Cifarelli, F. Cindolo, A. Contin, M. Corradi³, S. De Pasquale,
G. Iacobucci, A. Margotti, R. Nania, A. Polini, G. Sartorelli, A. Zichichi

University and INFN Bologna, Bologna, Italy ^e

D. Bartsch, I. Brock, S. Goers⁴, H. Hartmann, E. Hilger, H.-P. Jakob, M. Jüngst, O.M. Kind,
E. Paul⁵, R. Renner, U. Samson, V. Schönberg, R. Shehzadi, M. Wlasenko
Physikalisches Institut der Universität Bonn, Bonn, Germany ^b

N.H. Brook, G.P. Heath, J.D. Morris, T. Namsoo

H.H. Wills Physics Laboratory, University of Bristol, Bristol, United Kingdom ^m

M. Capua, S. Fazio, A. Mastroberardino, M. Schioppa, G. Susinno, E. Tassi
Calabria University, Physics Department and INFN, Cosenza, Italy ^e

J.Y. Kim⁶, K.J. Ma⁷

Chonnam National University, Kwangju, South Korea ^g

Z.A. Ibrahim, B. Kamaluddin, W.A.T. Wan Abdullah

Jabatan Fizik, Universiti Malaya, 50603 Kuala Lumpur, Malaysia ^r

Y. Ning, Z. Ren, F. Sciulli

Nevis Laboratories, Columbia University, Irvington on Hudson, New York 10027 ^o

J. Chwastowski, A. Eskreys, J. Figiel, A. Galas, M. Gil, K. Olkiewicz, P. Stopa, L. Zawiejski

*The Henryk Niewodniczanski Institute of Nuclear Physics, Polish Academy of Sciences,
Cracow, Poland* ⁱ

L. Adamczyk, T. Bołd, I. Grabowska-Bołd, D. Kisielewska, J. Lukasik, M. Przybycień,
L. Suszycki

*Faculty of Physics and Applied Computer Science, AGH-University of Science and Technology,
Cracow, Poland* ^p

A. Kotański⁸, W. Słomiński⁹

Department of Physics, Jagellonian University, Cracow, Poland

V. Adler⁴, U. Behrens, I. Bloch, C. Blohm, A. Bonato, K. Borras, R. Ciesielski, N. Coppoli, A. Dossanov, V. Drugakov, J. Fourletova, A. Geiser, D. Gladkov, P. Göttlicher¹⁰, I. Gregor, T. Haas, W. Hain, C. Horn¹¹, B. Kahle, I.I. Katkov, U. Klein¹², U. Kötz, H. Kowalski, E. Lobodzinska, B. Löhr, R. Mankel, I.-A. Melzer-Pellmann, S. Miglioranzi, A. Montanari, D. Notz, A.E. Nuncio-Quiroz, L. Rinaldi, I. Rubinsky, R. Santamarta, U. Schneekloth, A. Spiridonov¹³, H. Stadie, D. Szuba¹⁴, J. Szuba¹⁵, T. Theedt, G. Wolf, K. Wrona, C. Youngman, W. Zeuner

Deutsches Elektronen-Synchrotron DESY, Hamburg, Germany

W. Lohmann, S. Schlenstedt

Deutsches Elektronen-Synchrotron DESY, Zeuthen, Germany

G. Barbagli, E. Gallo, P. G. Pelfer

University and INFN, Florence, Italy ^e

A. Bamberger, D. Dobur, F. Karstens, N.N. Vlasov¹⁶

Fakultät für Physik der Universität Freiburg i.Br., Freiburg i.Br., Germany ^b

P.J. Bussey, A.T. Doyle, W. Dunne, J. Ferrando, M. Forrest, D.H. Saxon, I.O. Skillicorn

Department of Physics and Astronomy, University of Glasgow, Glasgow, United Kingdom ^m

I. Gialas¹⁷, K. Papageorgiou

Department of Engineering in Management and Finance, Univ. of Aegean, Greece

T. Gosau, U. Holm, R. Klanner, E. Lohrmann, H. Salehi, P. Schleper, T. Schörner-Sadenius, J. Sztuk, K. Wichmann, K. Wick

Hamburg University, Institute of Exp. Physics, Hamburg, Germany ^b

C. Foudas, C. Fry, K.R. Long, A.D. Tapper

Imperial College London, High Energy Nuclear Physics Group, London, United Kingdom ^m

M. Kataoka¹⁸, T. Matsumoto, K. Nagano, K. Tokushuku¹⁹, S. Yamada, Y. Yamazaki

Institute of Particle and Nuclear Studies, KEK, Tsukuba, Japan ^f

A.N. Barakbaev, E.G. Boos, N.S. Pokrovskiy, B.O. Zhautykov

Institute of Physics and Technology of Ministry of Education and Science of Kazakhstan, Almaty, Kazakhstan

D. Son

Kyungpook National University, Center for High Energy Physics, Daegu, South Korea ^g

J. de Favereau, K. Piotrzkowski

Institut de Physique Nucléaire, Université Catholique de Louvain, Louvain-la-Neuve, Belgium ^q

F. Barreiro, C. Glasman²⁰, M. Jimenez, L. Labarga, J. del Peso, E. Ron, M. Soares, J. Terrón, M. Zambrana

Departamento de Física Teórica, Universidad Autónoma de Madrid, Madrid, Spain ^l

F. Corriveau, C. Liu, R. Walsh, C. Zhou

Department of Physics, McGill University, Montréal, Québec, Canada H3A 2T8 ^a

T. Tsurugai

Meiji Gakuin University, Faculty of General Education, Yokohama, Japan ^f

A. Antonov, B.A. Dolgoshein, V. Sosnovtsev, A. Stifutkin, S. Suchkov

Moscow Engineering Physics Institute, Moscow, Russia ^j

R.K. Dementiev, P.F. Ermolov, L.K. Gladilin, L.A. Khein, I.A. Korzhavina, V.A. Kuzmin, B.B. Levchenko²¹, O.Yu. Lukina, A.S. Proskuryakov, L.M. Shcheglova, D.S. Zotkin, S.A. Zotkin

Moscow State University, Institute of Nuclear Physics, Moscow, Russia ^k

I. Abt, C. Büttner, A. Caldwell, D. Kollar, W.B. Schmidke, J. Sutiak

Max-Planck-Institut für Physik, München, Germany

G. Grigorescu, A. Keramidas, E. Koffeman, P. Kooijman, A. Pellegrino, H. Tiecke, M. Vázquez¹⁸, L. Wiggers

NIKHEF and University of Amsterdam, Amsterdam, Netherlands ^h

N. Brümmer, B. Bylsma, L.S. Durkin, A. Lee, T.Y. Ling

Physics Department, Ohio State University, Columbus, Ohio 43210 ⁿ

P.D. Allfrey, M.A. Bell, A.M. Cooper-Sarkar, A. Cottrell, R.C.E. Devenish, B. Foster, K. Korcsak-Gorzo, S. Patel, V. Roberfroid²², A. Robertson, P.B. Straub, C. Uribe-Estrada, R. Walczak

Department of Physics, University of Oxford, Oxford United Kingdom ^m

P. Bellan, A. Bertolin, R. Brugnera, R. Carlin, F. Dal Corso, S. Dusini, A. Garfagnini, S. Limentani, A. Longhin, L. Stanco, M. Turcato

Dipartimento di Fisica dell' Università and INFN, Padova, Italy ^e

B.Y. Oh, A. Raval, J. Ukleja²³, J.J. Whitmore²⁴

Department of Physics, Pennsylvania State University, University Park, Pennsylvania 16802 ^o

Y. Iga

Polytechnic University, Sagamihara, Japan ^f

G. D'Agostini, G. Marini, A. Nigro

Dipartimento di Fisica, Università 'La Sapienza' and INFN, Rome, Italy ^e

J.E. Cole, J.C. Hart

Rutherford Appleton Laboratory, Chilton, Didcot, Oxon, United Kingdom ^m

H. Abramowicz²⁵, A. Gabareen, R. Ingbir, S. Kananov, A. Levy

Raymond and Beverly Sackler Faculty of Exact Sciences, School of Physics, Tel-Aviv University, Tel-Aviv, Israel ^d

M. Kuze, J. Maeda

Department of Physics, Tokyo Institute of Technology, Tokyo, Japan ^f

R. Hori, S. Kagawa²⁶, N. Okazaki, S. Shimizu, T. Tawara

Department of Physics, University of Tokyo, Tokyo, Japan ^f

R. Hamatsu, H. Kaji²⁷, S. Kitamura²⁸, O. Ota, Y.D. Ri

Tokyo Metropolitan University, Department of Physics, Tokyo, Japan ^f

M.I. Ferrero, V. Monaco, R. Sacchi, A. Solano

Università di Torino and INFN, Torino, Italy ^e

M. Arneodo, M. Ruspa

Università del Piemonte Orientale, Novara, and INFN, Torino, Italy ^e

S. Fourletov, J.F. Martin

Department of Physics, University of Toronto, Toronto, Ontario, Canada M5S 1A7 ^a

S.K. Boulle¹⁷, J.M. Butterworth, C. Gwenlan²⁹, T.W. Jones, J.H. Loizides, M.R. Sutton²⁹, M. Wing

Physics and Astronomy Department, University College London, London, United Kingdom ^m

B. Brzozowska, J. Ciborowski³⁰, G. Grzelak, P. Kulinski, P. Łužniak³¹, J. Malka³¹, R.J. Nowak, J.M. Pawlak, T. Tymieniecka, A. Ukleja, A.F. Żarnecki

Warsaw University, Institute of Experimental Physics, Warsaw, Poland

M. Adamus, P. Plucinski³²

Institute for Nuclear Studies, Warsaw, Poland

Y. Eisenberg, I. Giller, D. Hochman, U. Karshon, M. Rosin

Department of Particle Physics, Weizmann Institute, Rehovot, Israel ^c

E. Brownson, T. Danielson, A. Everett, D. Kçira, D.D. Reeder⁵, P. Ryan, A.A. Savin, W.H. Smith, H. Wolfe

Department of Physics, University of Wisconsin, Madison, Wisconsin 53706, USA ⁿ

S. Bhadra, C.D. Catterall, Y. Cui, G. Hartner, S. Menary, U. Noor, J. Standage, J. Whyte

Department of Physics, York University, Ontario, Canada M3J 1P3 ^a

¹ supported by DESY, Germany

² also affiliated with University College London, UK

³ also at University of Hamburg, Germany, Alexander von Humboldt Fellow

⁴ self-employed

⁵ retired

⁶ supported by Chonnam National University in 2005

⁷ supported by a scholarship of the World Laboratory Björn Wiik Research Project

⁸ supported by the research grant no. 1 P03B 04529 (2005-2008)

⁹ This work was supported in part by the Marie Curie Actions Transfer of Knowledge project COCOS (contract MTKD-CT-2004-517186)

¹⁰ now at DESY group FEB, Hamburg, Germany

¹¹ now at Stanford Linear Accelerator Center, Stanford, USA

¹² now at University of Liverpool, UK

¹³ also at Institut of Theoretical and Experimental Physics, Moscow, Russia

¹⁴ also at INP, Cracow, Poland

¹⁵ on leave of absence from FPACS, AGH-UST, Cracow, Poland

¹⁶ partly supported by Moscow State University, Russia

¹⁷ also affiliated with DESY

¹⁸ now at CERN, Geneva, Switzerland

¹⁹ also at University of Tokyo, Japan

²⁰ Ramón y Cajal Fellow

²¹ partly supported by Russian Foundation for Basic Research grant no. 05-02-39028-NSFC-a

²² EU Marie Curie Fellow

²³ partially supported by Warsaw University, Poland

²⁴ This material was based on work supported by the National Science Foundation, while working at the Foundation.

²⁵ also at Max Planck Institute, Munich, Germany, Alexander von Humboldt Research Award

²⁶ now at KEK, Tsukuba, Japan

²⁷ now at Nagoya University, Japan

²⁸ Department of Radiological Science

²⁹ PPARC Advanced fellow

³⁰ also at Lódź University, Poland

³¹ Lódź University, Poland

³² supported by the Polish Ministry for Education and Science grant no. 1 P03B 14129

[†] deceased

- ^a supported by the Natural Sciences and Engineering Research Council of Canada (NSERC)
- ^b supported by the German Federal Ministry for Education and Research (BMBF), under contract numbers HZ1GUA 2, HZ1GUB 0, HZ1PDA 5, HZ1VFA 5
- ^c supported in part by the MINERVA Gesellschaft für Forschung GmbH, the Israel Science Foundation (grant no. 293/02-11.2) and the U.S.-Israel Binational Science Foundation
- ^d supported by the German-Israeli Foundation and the Israel Science Foundation
- ^e supported by the Italian National Institute for Nuclear Physics (INFN)
- ^f supported by the Japanese Ministry of Education, Culture, Sports, Science and Technology (MEXT) and its grants for Scientific Research
- ^g supported by the Korean Ministry of Education and Korea Science and Engineering Foundation
- ^h supported by the Netherlands Foundation for Research on Matter (FOM)
- ⁱ supported by the Polish State Committee for Scientific Research, grant no. 620/E-77/SPB/DESY/P-03/DZ 117/2003-2005 and grant no. 1P03B07427/2004-2006
- ^j partially supported by the German Federal Ministry for Education and Research (BMBF)
- ^k supported by RF Presidential grant N 8122.2006.2 for the leading scientific schools and by the Russian Ministry of Education and Science through its grant Research on High Energy Physics
- ^l supported by the Spanish Ministry of Education and Science through funds provided by CICYT
- ^m supported by the Particle Physics and Astronomy Research Council, UK
- ⁿ supported by the US Department of Energy
- ^o supported by the US National Science Foundation. Any opinion, findings and conclusions or recommendations expressed in this material are those of the authors and do not necessarily reflect the views of the National Science Foundation.
- ^p supported by the Polish Ministry of Science and Higher Education as a scientific project (2006-2008)
- ^q supported by FNRS and its associated funds (IISN and FRIA) and by an Inter-University Attraction Poles Programme subsidised by the Belgian Federal Science Policy Office
- ^r supported by the Malaysian Ministry of Science, Technology and Innovation/Akademi Sains Malaysia grant SAGA 66-02-03-0048

1 Introduction

In diffractive electron-proton scattering, the proton loses a small fraction of its energy and either emerges from the scattering intact, $ep \rightarrow eXp$, or dissociates into a low-mass state N , $ep \rightarrow eXN$. A large gap in rapidity separates the hadronic-state X with invariant-mass M_X and the final-state proton (or N).

In the framework of Regge phenomenology [1], diffractive interactions are ascribed to the exchange of a trajectory with vacuum quantum numbers, the Pomeron trajectory. In quantum chromodynamics (QCD), the diffractive factorisation theorem [2–5] states that the diffractive cross section, in the presence of a hard scale, can be expressed as the convolution of universal partonic cross sections and a specific type of parton distribution function (PDF), the diffractive PDF (dPDF). Diffractive PDFs are interpreted as conditional probabilities to find a parton in the proton when the final state contains a fast forward proton. The dPDFs [6–9] have been determined from the HERA inclusive measurements of the diffractive structure function (F_2^D), defined in analogy with the proton structure function (F_2) [10], and can be used as input for calculations of different diffractive processes, for example at the Tevatron and LHC [11].

Diffractive collisions, producing hadronic-states X including a $c\bar{c}$ pair, are a particularly interesting component of diffractive ep interactions. The charm-quark mass provides a hard scale, ensuring the applicability of perturbative QCD even for small photon virtualities (photoproduction). At leading order (LO) of QCD, two types of photoproduction processes can be distinguished: direct and resolved photon processes. Charm production mainly proceeds via direct photon reactions, in which the exchanged photon participates as a point-like particle, directly interacting with a gluon from the incoming proton (photon-gluon fusion, Fig. 1). Thus, diffractive charm production is directly sensitive to the gluon content of the diffractive exchange. In the resolved photon processes, the photon behaves as a hadron-like source of partons, one of which interacts with a parton from the initial proton. Further interactions between partons from the photon and the proton may fill the rapidity gap, leading to a suppression of the observed cross sections in diffractive photoproduction. For example, an eikonal model [13] predicts a cross-section suppression by about a factor of three for diffractive resolved photoproduction at HERA. A similar mechanism was proposed to explain the rate of hard diffractive events at the Tevatron, which is lower than the expectations based on the dPDFs measured at HERA [14].

This paper presents a study of diffractive charm production, $ep \rightarrow eXp \rightarrow eD^*X'p$, with exchanged-photon virtuality $Q^2 < 1 \text{ GeV}^2$. The production of charm was tagged by identification of a $D^{*\pm}(2010)$ meson in the final state¹. The measurement is based on a

¹ From now on, the notation D^* will be used for both D^{*+} and D^{*-} .

sample of events with a large gap in pseudorapidity between the proton and the produced hadronic system. Diffractive charm production was measured previously at HERA in deep inelastic scattering (DIS) for photon virtualities above 1.5 GeV^2 [15–18]. Recently, the H1 Collaboration has reported a measurement of diffractive charm photoproduction with $Q^2 < 0.01 \text{ GeV}^2$ [16]. The measurement reported here is performed with about six times larger statistics and in a larger kinematic range than the H1 results.

2 Experimental set-up

This measurement is based on the data taken with the ZEUS detector at the ep collider HERA in 1998–2000, when electrons or positrons of 27.5 GeV were collided with protons of 920 GeV. The sample used for this study corresponds to an integrated luminosity $\mathcal{L} = 78.6 \pm 1.8 \text{ pb}^{-1}$ (13.6 pb^{-1} and 65.1 pb^{-1} for the e^-p and e^+p samples, respectively²).

A detailed description of the ZEUS detector can be found elsewhere [19]. Only a brief outline of the detector components most relevant to this analysis is given here.

Charged particles are tracked in the central tracking detector (CTD) [20], which operates in a magnetic field of 1.43 T, provided by a thin super-conducting coil. The CTD consists of 72 cylindrical drift chamber layers, arranged in 9 superlayers, covering the polar angle region³ $15^\circ < \theta < 164^\circ$. The transverse-momentum resolution for full-length tracks is $\sigma(p_T)/p_T = 0.0058p_T \oplus 0.0065 \oplus 0.0014/p_T$, with p_T in GeV.

The high-resolution uranium–scintillator calorimeter (CAL) [21] consists of three parts: the forward (FCAL), the barrel (BCAL) and the rear (RCAL) calorimeters. Each part is subdivided transversely into towers and longitudinally into one electromagnetic section and either one (in RCAL) or two (in BCAL and FCAL) hadronic sections. The smallest subdivision of the calorimeter is called a cell. The CAL energy resolutions, as measured under test-beam conditions, are $\sigma(E)/E = 0.18/\sqrt{E}$ for electrons and $\sigma(E)/E = 0.35/\sqrt{E}$ for hadrons, with E in GeV.

In 1998–2000, the forward plug calorimeter (FPC) [22] was installed in the $20 \times 20 \text{ cm}^2$ beam hole of the FCAL with a small hole of radius 3.15 cm in the centre to accommodate the beam pipe. The FPC increased the forward calorimetric coverage by about one unit in pseudorapidity to $\eta \leq 5$.

The luminosity was measured from the rate of the bremsstrahlung process $ep \rightarrow e\gamma p$. The

² From now on, the word “electron” will be used as a generic term for both electrons and positrons.

³ The ZEUS coordinate system is a right-handed Cartesian system, with the Z axis pointing in the proton beam direction, referred to as the “forward direction”, and the X axis pointing left towards the centre of HERA. The coordinate origin is at the nominal interaction point.

bremsstrahlung photons were measured with a lead–scintillator calorimeter [23] placed in the HERA tunnel at $Z = -107$ m.

3 Kinematics and reconstruction of variables

Diffractive photoproduction in ep scattering (Fig. 1),

$$e(e) + p(p) \rightarrow e(e') + X(X) + p(p'),$$

is described in terms of the four-momenta e, e' of the beam and scattered electrons, p, p' of the beam and scattered protons and X of the hadronic system. The following kinematic variables are defined: the photon virtuality, $Q^2 = -q^2$, where $q = e - e'$, the squared photon-proton centre-of-mass energy, $W^2 = (p + q)^2$, and the fraction of the electron energy transferred to the proton in its rest frame,

$$y = \frac{p \cdot q}{p \cdot e} \simeq \frac{W^2}{2p \cdot e}.$$

The reaction can be considered to proceed through the interaction of the virtual photon with the diffractive exchange (Pomeron, \mathcal{IP}). This process is described by the invariant mass, M_X , of the hadronic system X and the fraction of the proton momentum

$$x_{\mathcal{IP}} = \frac{(p - p') \cdot q}{p \cdot q}$$

carried by the diffractive exchange.

The variables W , M_X and $x_{\mathcal{IP}}$ were reconstructed from the hadronic final state, using a combination of track and calorimeter information that optimises the resolution of the reconstructed kinematic variables. The selected tracks and calorimeter clusters are referred to as energy-flow objects (EFO) [24]. The Jacquet–Blondel formula [25]

$$W_{\text{JB}} = \sqrt{2E_p(E - P_Z)}$$

was used to reconstruct W , where E_p is the proton beam energy and

$$E - P_Z = \sum_i (E_i - P_{Z_i}) .$$

The invariant mass of the diffractively produced system was calculated from

$$M_X^2 = \left(\sum_i E_i \right)^2 - \left(\sum_i P_{X_i} \right)^2 - \left(\sum_i P_{Y_i} \right)^2 - \left(\sum_i P_{Z_i} \right)^2 .$$

The sums in the above equations run over the energies E_i and momentum components P_{X_i} , P_{Y_i} and P_{Z_i} of all EFOs.

The variable x_{p} was reconstructed from

$$x_{\text{p}} = \frac{M_X^2}{W^2},$$

which is derived neglecting the photon virtuality ($Q^2 \simeq 0$ for the case of photoproduction), the square of the four-momentum transfer at the proton vertex ($t = -(p - p')^2$), and the mass of the proton.

In addition, the inelasticity $z(D^*)$ was defined as

$$z(D^*) = \frac{p \cdot p(D^*)}{p \cdot q},$$

where $p(D^*)$ is the four-momentum of the D^* meson. In the proton rest frame, $z(D^*)$ is the fraction of the photon energy carried by the D^* meson. This variable was reconstructed as

$$z(D^*) = \frac{(E - P_Z)_{D^*}}{(E - P_Z)},$$

where $(E - P_Z)_{D^*}$ was calculated using the momentum of the D^* meson.

The measured values of the variables W , $z(D^*)$, M_X and x_{p} were corrected for energy losses in the inactive material of the ZEUS detector and for the loss of any particle down the beam pipe using Monte Carlo (MC) simulations. All variables were reconstructed with an accuracy of better than 15% over the ranges considered.

4 Theoretical predictions

4.1 Monte Carlo simulations

Monte Carlo simulations were used to calculate the acceptances, to evaluate correction factors for the selection inefficiencies and resolutions of the ZEUS detector and to estimate the background.

The MC generator RAPGAP 2.08/18 [26] was used to simulate diffractive photoproduction of D^* mesons. The simulation was performed in the framework of the resolved-Pomeron model [12]. The cross section is proportional to the diffractive proton structure function, F_2^D , which is parameterised by the product of the probability of the Pomeron emission (the so-called Pomeron flux factor) and the structure function of the Pomeron. The parameterisation of the Pomeron flux factor by Streng and Berger [27] was used along with

the Pomeron structure function obtained by the H1 Collaboration (H1Fit2 LO) [28]. The contribution of the sub-leading Regge trajectory (the Reggeon), which is only significant for $x_{\mathbb{P}} > 0.01$, was also included.

The ep interactions were modelled using both direct and resolved photon processes. The resolved photon component, which amounts to about 35% of the total sample, is dominated by heavy-flavour excitation, in which a charm quark from the photon participates in the hard scattering. To simulate resolved photon processes, the GRV-G-LO [29] set of photon parton densities was used. The simulation of charm production was performed with the leading-order matrix elements. Higher-order QCD effects were approximated by parton showers, based on the leading logarithm (LL) DGLAP splitting functions [30]. Contributions from bottom production with subsequent decay into a final state with D^* were also simulated. The bottom contribution, as predicted by the MC calculations, is not sizeable in any part of the kinematic range and corresponds to 2-3% of the total sample. The masses of the heavy quarks were set to $m_c = 1.5$ GeV for charm and $m_b = 4.75$ GeV for bottom.

The MC generators PYTHIA 6.156 [31] and HERWIG 6.301 [32] were used to model the non-diffractive photoproduction of the D^* mesons. The CTEQ5L parameterisation [33] was used in both generators for the proton PDFs.

The hadronisation process was simulated with the Lund string model [31] in the RAPGAP and PYTHIA MCs, and according to a cluster hadronisation model [34] in HERWIG.

The generated Monte Carlo events were passed through the standard simulation of the ZEUS detector, based on the GEANT 3.13 simulation program [35], and through the ZEUS trigger simulation package [36]. The simulated detector responses were then subjected to the same reconstruction and analysis procedures as the data. For the determination of the acceptance and correction factors, the generated RAPGAP events were re-weighted in the variables M_X and $z(D^*)$, and the generated PYTHIA and HERWIG events were re-weighted in the variables $p_T(D^*)$ and $\eta(D^*)$ to improve the description of the shapes of the measured distributions.

4.2 NLO QCD calculations

The cross sections for diffractive photoproduction of D^* mesons were calculated at the next-to-leading order (NLO) in α_s , the strong coupling constant, using the fixed-flavour-number scheme, in which only light flavours are active in the PDFs and the heavy quarks are generated by the hard interaction. The calculation was performed with the FMNR code in the double-differential mode [37,38]. The Weizsäcker-Williams approximation [39] was used to obtain the virtual photon spectrum for electroproduction with small photon

virtualities. Diffractive PDFs were used instead of the conventional proton PDFs. The three sets of dPDFs used in the calculations were derived from NLO QCD DGLAP fits to the HERA data on diffractive deep inelastic scattering: the H1 2006 Fit A, Fit B [6] and the ZEUS LPS+charm Fit [7] diffractive PDFs. In the ZEUS LPS+charm fit, the diffractive DIS data were combined with the results on diffractive charm production in DIS [18] to better constrain the gluon contribution. The Reggeon contribution, which amounts to less than 2% for $x_{\text{IP}} = 0.01$ and grows up to $\sim 15\%$ at $x_{\text{IP}} = 0.035$, was not included. To account for the proton-dissociative contribution, present in the H1 2006 fits, the corresponding predictions were multiplied by the factor 0.81 [6].

The calculations were performed with $\alpha_s(M_Z) = 0.118 \text{ GeV}$ [40] and $m_c = 1.45 \text{ GeV}$, the same values used in the QCD fits to the HERA data. The fraction of charm quarks hadronising as D^* mesons was set to $f(c \rightarrow D^*) = 0.238$ [41]. The Peterson parameterisation [42] was used for the charm fragmentation with the Peterson parameter $\epsilon = 0.035$, obtained in an NLO fit [43] to ARGUS data [44]. The central NLO QCD predictions were obtained with the renormalisation and factorisation scales set to $\mu_R = \mu_F = \mu \equiv \sqrt{m_c^2 + 0.5 \cdot [p_T^2(c) + p_T^2(\bar{c})]}$. Here, $p_T(c)$ and $p_T(\bar{c})$ are the transverse momenta of the charm and anti-charm quarks. The uncertainties of the calculations were estimated by varying the renormalisation and factorisation scales simultaneously with the charm mass to $\mu_R = \mu_F = 0.5 \cdot \mu$, $m_c = 1.25 \text{ GeV}$ and to $\mu_R = \mu_F = 2 \cdot \mu$, $m_c = 1.65 \text{ GeV}$. Uncertainties on the dPDFs were not included.

The NLO predictions are given by the sum of point-like and hadron-like processes, the NLO analogues of the direct and resolved photon processes defined at LO. In all NLO calculations, the AFG-G-HO parameterisation [45] was taken for the photon PDFs. The hadron-like processes, in which the photon behaves as a source of light partons, contribute about 10% of the FMNR cross section. The dependence on the photon PDFs was checked by using the GRV-G-HO parameterisation [46] and was found to be negligible. It should be noted that the NLO diagrams in which the photon splits into a low-mass pair of c and \bar{c} quarks, one of which interacts with a gluon from the proton, are considered as point-like photon processes in FMNR while they are effectively included in Rapgap as resolved-photon processes with heavy-flavour excitation.

In the calculations of the inclusive D^* photoproduction cross sections, the CTEQ5M parameterisation [33] with the default value of the QCD parameter ($\Lambda_{\text{QCD}}^{(5)} = 226 \text{ MeV}$) was taken for the PDFs of the proton.

5 Event selection and reconstruction of $D^{*\pm}$ mesons

5.1 Event selection

The events were selected online with a three-level trigger system [19, 36]. At the first- and second-level triggers, data from CAL and CTD were used to select ep collisions and to reject non- ep backgrounds. At the third level, the full event information was available and at least one reconstructed D^* candidate (see below) was required. The efficiency of the online D^* reconstruction, relative to the efficiency of the offline reconstruction, was above 95%.

Photoproduction events were selected offline by requiring that no scattered electron was identified in the CAL [47]. After correcting for detector effects, the most important of which were energy losses in the inactive material in front of the CAL and particle losses in the beam pipe [47, 48], events were selected in the interval $130 < W < 300 \text{ GeV}$ ($0.17 < y < 0.89$). The lower limit was set by the trigger requirements, while the upper limit was imposed to suppress any remaining events from deep inelastic scattering. Under these conditions, the photon virtuality is below 1 GeV^2 . The median Q^2 value was estimated from a MC simulation to be about $3 \times 10^{-4} \text{ GeV}^2$.

5.2 Reconstruction and selection of $D^{*\pm}(2010)$ mesons

The $D^{*}(2010)$ mesons were reconstructed from the decay $D^* \rightarrow (D^0 \rightarrow K\pi)\pi_s$ by means of the mass-difference method using charged tracks measured by the CTD. The π_s particle from the D^* decay is known as the “soft” pion because its momentum value is limited by the small difference between the masses of the D^* and D^0 mesons. To ensure a good efficiency and a good momentum resolution, tracks were required to have $p_T > 0.12 \text{ GeV}$ and to reach at least the third CTD superlayer.

To reconstruct a D^* candidate [49], two tracks of opposite charges were combined into a $(K\pi)$ pair forming a D^0 candidate. As kaons and pions were not identified, the mass of a charged kaon and a charged pion was assigned to each track in turn.

Similarly, to form a “right-charge” track combination for a D^* candidate, each $(K\pi)$ pair was combined with a third track (π_s), which had the charged-pion mass assigned and charge opposite to that of the K meson in the $(K\pi)$ pair. To reduce the combinatorial background, the tracks for the above combinations were selected with transverse momenta as follows: $p_T(K) > 0.5 \text{ GeV}$, $p_T(\pi) > 0.5 \text{ GeV}$ and $p_T(\pi_s) > 0.12 \text{ GeV}$. The $p_T(\pi_s)$ cut was raised to 0.25 GeV for a data sub-sample, corresponding to an integrated luminosity of $16.9 \pm 0.4 \text{ pb}^{-1}$, for which the reconstruction efficiency of

low momentum tracks was smaller due to the operating conditions of the CTD [50]. The D^* -meson candidates were accepted provided the invariant-mass value $M(K\pi)$ was consistent with the nominal $M(D^0)$ mass given by the PDG [40]. To take the mass resolutions into account, the following requirements were applied, depending on $p_T(D^*)$, the transverse momentum of the D^* meson [51]:

$$\begin{aligned} 1.82 < M(K\pi) < 1.91 \text{ GeV} & \quad \text{for} \quad p_T(D^*) < 3.25 \text{ GeV}, \\ 1.81 < M(K\pi) < 1.92 \text{ GeV} & \quad \text{for} \quad 3.25 < p_T(D^*) < 5 \text{ GeV}, \\ 1.80 < M(K\pi) < 1.93 \text{ GeV} & \quad \text{for} \quad 5 < p_T(D^*) < 8 \text{ GeV} \text{ and} \\ 1.79 < M(K\pi) < 1.94 \text{ GeV} & \quad \text{for} \quad p_T(D^*) > 8 \text{ GeV}. \end{aligned}$$

To suppress the combinatorial background further, the transverse momentum of the D^* candidates was required to exceed 1.9 GeV and a cut on the ratio $p_T(D^*)/E_T^{\theta>10^\circ} > 0.1$ was applied. Here $E_T^{\theta>10^\circ}$ is the transverse energy measured in the CAL outside a cone of $\theta = 10^\circ$ around the forward direction. Monte Carlo studies showed that such a cut removes a significant fraction of the background whilst preserving most of the produced D^* mesons. The measurements were restricted to the pseudorapidity range $|\eta(D^*)| < 1.6$, where the CTD acceptance is high. A clear signal was observed in the resulting mass difference $\Delta M = M(K\pi\pi_s) - M(K\pi)$ distribution (not shown) at the nominal value.

To determine the number of D^* mesons in the signal range, $0.1435 < \Delta M < 0.1475$ GeV, the combinatorial background was modelled by “wrong-charge” track combinations and subtracted, after normalisation to the “right-charge” distribution in the range $0.15 < \Delta M < 0.17$ GeV. A “wrong-charge” track combination for a $(K\pi)$ pair was defined as two tracks of the same charge with a soft pion (π_s) of the opposite charge. This subtraction yielded a signal of 12482 ± 208 inclusive D^* mesons.

5.3 Selection of diffractive events

Diffractive events were identified by the presence of a large rapidity gap (LRG) between the beam pipe, through which the scattered proton escaped detection, and the hadronic-system X [52]. The events with a LRG were selected by applying a cut on the pseudorapidity η_{\max} of the most forward EFO with an energy greater than 400 MeV.

Figure 2a compares the measured η_{\max} distribution for all photoproduced D^* events (after “wrong-charge” background subtraction) to a sum of the distributions from diffractive (RAPGAP) and non-diffractive (PYTHIA) MC samples. The relative proportions of the two MC samples in the sum were chosen to give the best description of the shape of the data. The measured distribution shows two structures. The plateau at $\eta_{\max} < 3$ is populated predominantly by diffractive events, while the peak around $\eta_{\max} \sim 3.5$ originates mainly

from non-diffractive events. To select diffractive events, while rejecting the majority of the non-diffractive events, the energy deposited in the FPC was required to be consistent with zero ($E_{\text{FPC}} < 1.5 \text{ GeV}$). Comparison between the η_{max} distributions of these data and MC events (Fig. 2b) confirms the considerable reduction of non-diffractive events in the sample. To further reduce the fraction of non-diffractive events, a cut $\eta_{\text{max}} < 3$ was applied. This cut ensures a gap of at least two units of pseudorapidity with respect to the edge of the forward calorimetric coverage provided by the FPC. A cut in η_{max} correlates with the range of accessible x_{P} values. The requirement $\eta_{\text{max}} < 3$ restricts the measurement to $x_{\text{P}} < 0.035$.

After the above selections, a signal of 458 ± 30 D^* mesons was found in the ΔM distribution (Fig. 3) for diffractive photoproduction in the range $x_{\text{P}} < 0.035$. In order to reduce the contributions from the Reggeon exchange and non-diffractive background, the selection was also performed in the restricted range $x_{\text{P}} < 0.01$, where 204 ± 20 D^* mesons were observed.

From the comparison between the measured and MC η_{max} distributions (see above and Fig. 2a), normalisation factors were obtained for the diffractive and the non-diffractive MC samples. These normalisation factors were then used to evaluate the total and differential fractions (f_{nd}) of residual non-diffractive events in the range $\eta_{\text{max}} < 3$ and to correct all the measured distributions for this background bin-by-bin. The total fraction $f_{\text{nd}} = 3.3\%$ was evaluated using the PYTHIA MC sample. Similar calculations were performed with the HERWIG MC sample (total $f_{\text{nd}} = 15.5\%$) for the purpose of systematic uncertainty evaluation.

The proton-dissociative events, $ep \rightarrow eXN$, can also satisfy the requirements $\eta_{\text{max}} < 3$ and $E_{\text{FPC}} < 1.5 \text{ GeV}$ if the proton-dissociative system, N , has an invariant mass small enough to pass undetected through the forward beam-pipe. The fraction (f_{pd}) of background proton-dissociative events was measured previously to be $f_{\text{pd}} = 16 \pm 4(\text{syst.})\%$ [18].

6 Systematic uncertainties

The cross section uncertainties for $x_{\text{P}} < 0.035$ and $x_{\text{P}} < 0.01$ were determined separately. The following sources of systematic uncertainty were taken into account (uncertainties for the range $x_{\text{P}} < 0.01$ are given in brackets):

- the CAL simulation uncertainty was determined by varying the CAL energy scale by $\pm 2\%$ and the CAL energy resolution by $\pm 20\%$ of its value. The CAL first-level trigger efficiencies were varied by their uncertainty. These variations resulted in a combined $^{+1.8}_{-1.5} (\pm 2.3)\%$ uncertainty on the cross section;

- the tracking-simulation uncertainties, which were obtained by varying all momenta by $\pm 0.3\%$ (magnetic field uncertainty) and by changing the track momentum and angular resolutions by $^{+20}_{-10}\%$ of their values, yielded a combined cross-section uncertainty of $^{+3.5}_{-1.9} (^{+3.2}_{-3.3})\%$;
- the uncertainty in the subtraction of the combinatorial background was estimated by tightening separately by 2 MeV the lower and the upper boundary of the region in which the “wrong-charge” background was normalised. This contributed $+0.2 (-0.5)\%$ to the cross-section uncertainty;
- the uncertainty in the FPC energy scale, evaluated by $\pm 10\%$ variations of the FPC energy in the MC, gave a systematic uncertainty of $^{+0.2}_{-0.4} (-0.2)\%$;
- the uncertainty in the selection of diffractive events was evaluated by varying the E_{FPC} cut by ± 0.5 GeV, which yielded a cross-section uncertainty of $^{+0.0}_{-0.9} (^{+0.2}_{-0.3})\%$, and the η_{max} cut by ± 0.2 , which yielded a cross-section uncertainty of $^{+6.3}_{-1.9} (^{+2.6}_{-0.0})\%$. The resulting uncertainty on the selection of diffractive events was $^{+6.3}_{-2.1} (^{+2.6}_{-0.3})\%$;
- the uncertainty from the model dependence of the acceptance corrections was determined by varying the re-weighting factors of the MC samples by $\pm 20\%$ of their values. The resulting cross-section uncertainty was $^{+1.5}_{-1.4} (^{+3.2}_{-3.3})\%$;
- the uncertainty from the model dependence of the non-diffractive event rejection was determined using HERWIG instead of PYTHIA, yielding a cross-section variation of $-11.9 (-6.8)\%$.

The above systematic uncertainties were added in quadrature to determine the total systematic uncertainty.

The overall normalisation uncertainties due to the subtraction of the proton dissociation ($\pm 4.8\%$), the luminosity measurement ($\pm 2.2\%$) and the D^* and D^0 decay branching ratios ($\pm 2\%$) were not included in the quoted systematic uncertainty.

7 Results

7.1 Cross sections

The differential cross section for $ep \rightarrow eD^*X'p$ in a given variable ξ was calculated from

$$\frac{d\sigma}{d\xi} = \frac{N_{D^*} \cdot (1 - f_{\text{nd}}) \cdot (1 - f_{\text{pd}})}{\mathcal{A} \cdot \mathcal{L} \cdot \mathcal{B} \cdot \Delta\xi},$$

where N_{D^*} is the number of D^* mesons observed in a bin of size $\Delta\xi$. The overall acceptance was $\mathcal{A} = 13.9\%$. The combined $D^* \rightarrow (D^0 \rightarrow K\pi)\pi_s$ decay branching ratio is $\mathcal{B} = 0.0257 \pm 0.0005$ [40].

The cross sections for diffractive D^* -meson photoproduction were measured in the kinematic range $Q^2 < 1 \text{ GeV}^2$, $130 < W < 300 \text{ GeV}$ ($0.17 < y < 0.89$), $p_T(D^*) > 1.9 \text{ GeV}$, $|\eta(D^*)| < 1.6$ and $x_{\text{F}} < 0.035$. No restriction in t was applied. The cross section, integrated over this range, is

$$\sigma_{ep \rightarrow eD^*X'p}(x_{\text{F}} < 0.035) = 1.49 \pm 0.11(\text{stat.})^{+0.11}_{-0.19}(\text{syst.}) \pm 0.07(\text{p.d.}) \text{ nb.}$$

The last uncertainty is due to the subtraction of the proton-dissociative background (see Section 5.3).

The measurement was also repeated in the narrower range $x_{\text{F}} < 0.01$, where the non-diffractive background admixture is smaller and the Reggeon contribution is expected to be negligible. The cross section integrated over the above kinematic region but for $x_{\text{F}} < 0.01$ is

$$\sigma_{ep \rightarrow eD^*X'p}(x_{\text{F}} < 0.01) = 0.63 \pm 0.07(\text{stat.})^{+0.04}_{-0.06}(\text{syst.}) \pm 0.03(\text{p.d.}) \text{ nb.}$$

For both x_{F} ranges, the differential cross sections, measured as functions of the variables x_{F} , M_X , $p_T(D^*)$, $\eta(D^*)$, $z(D^*)$ and W , are presented in Tables 1-4 and Figs. 4-7.

Figure 4 compares the measured cross sections to the expectations from the resolved-Pomeron model calculated by means of the RAPGAP MC program without re-weighting (Section 4.1). To compare the shapes with the measured cross sections, the model prediction was normalised by a factor 0.34. Reasonable agreement between the shapes of the calculated and measured differential cross sections is observed. The relative contribution of resolved photon processes predicted by RAPGAP increases towards forward $\eta(D^*)$, small $z(D^*)$ and large M_X .

Figures 5-7 compare the measurements to the three sets of NLO predictions obtained from the FMNR calculations using the H1 2006 Fit A, Fit B and ZEUS LPS+charm Fit dPDFs. The estimated calculation uncertainties (see Section 4.2) are shown as the shaded band only for H1 2006 Fit A and are similar for other calculations. The uncertainties of the NLO QCD predictions are larger than the experimental ones in most bins.

The NLO QCD calculations reproduce the x_{F} differential cross section (Fig. 5), in both shape and normalisation. A similar agreement between the calculations and the data is seen in Figs. 6 and 7 for the $p_T(D^*)$, $\eta(D^*)$, M_X and W differential cross sections in both ranges $x_{\text{F}} < 0.035$ and $x_{\text{F}} < 0.01$. The shapes of the differential distributions $d\sigma/dz(D^*)$ are not well reproduced by the NLO calculations. A better shape description of the $z(D^*)$ distributions is provided by RAPGAP (Fig. 4). The agreement between the NLO QCD predictions and the data supports the validity of the QCD factorisation theorem in diffraction, implying the universality of diffractive PDFs. However, given the

large experimental and theoretical uncertainties and the small hadron-like contribution expected by the NLO calculations, a suppression of the hadron-like component cannot be excluded.

7.2 Fraction of $D^{*\pm}$ meson diffractive photoproduction

The fraction of the diffractive to the inclusive ($ep \rightarrow eD^*Y$) photoproduction cross sections for D^* mesons was evaluated as

$$\mathcal{R}_D(D^*) = \frac{\sigma_{ep \rightarrow eD^*X'p}(x_{IP} < 0.035)}{\sigma_{ep \rightarrow eD^*Y}}.$$

In the kinematic region $Q^2 < 1 \text{ GeV}^2$, $130 < W < 300 \text{ GeV}$ ($0.17 < y < 0.89$), $p_T(D^*) > 1.9 \text{ GeV}$ and $|\eta(D^*)| < 1.6$, diffractive production for $x_{IP} < 0.035$ contributes

$$\mathcal{R}_D(D^*) = 5.7 \pm 0.5(\text{stat.})^{+0.4}_{-0.7}(\text{syst.}) \pm 0.3(\text{p.d.})\%$$

to the inclusive D^* photoproduction cross section. Systematic uncertainty partly cancel in this ratio. The residual systematic uncertainty is dominated by the measurement of the diffractive cross section. For the inclusive cross sections, the acceptance corrections were estimated with HERWIG. The difference with respect to PYTHIA was used as a systematic check.

This fraction \mathcal{R}_D agrees with the values measured at HERA for diffractive DIS in similar kinematic ranges [15, 17, 18]. As shown in Fig. 8, \mathcal{R}_D is approximately independent of Q^2 .

The differential dependences of the fraction \mathcal{R}_D on $p_T(D^*)$, $\eta(D^*)$, $z(D^*)$ and W are shown in Tables 3 and 4 and Fig. 9. Similar to the measurement in diffractive deep inelastic scattering [18], the fraction of the diffractive contribution decreases with increasing $p_T(D^*)$ and $\eta(D^*)$. The value of \mathcal{R}_D shows no strong dependence on either W or $z(D^*)$.

The NLO QCD predictions for \mathcal{R}_D were obtained as the ratio of the diffractive cross section, calculated with the H1 2006 or ZEUS LPS+charm dPDFs, and the inclusive cross section, obtained with the CTEQ5M proton PDFs. The calculated ratios reproduce the measured dependence of \mathcal{R}_D on the kinematic variables well both in shape and normalisation (Fig. 9), supporting diffractive QCD factorisation.

8 Conclusions

Diffractive cross sections and their fraction of the total photoproduction cross section of $D^{*\pm}(2010)$ mesons have been measured with the ZEUS detector at HERA

using an integrated luminosity of 78.6 pb^{-1} . The D^* mesons were reconstructed with $p_T > 1.9 \text{ GeV}$ and $|\eta| < 1.6$. The measurements have been performed in the kinematic region $Q^2 < 1 \text{ GeV}^2$, $130 < W < 300 \text{ GeV}$ ($0.17 < y < 0.89$), for the two ranges $x_P < 0.035$ and $x_P < 0.01$.

The measured differential cross sections and the fraction of the inclusive photoproduction of $D^{*\pm}$ mesons due to diffractive exchange have been compared to the predictions of NLO QCD calculations using available parameterisations of diffractive PDFs. The NLO predictions based on H1 2006 fits A and B as well as the ZEUS LPS+charm fit are consistent with the data. The measured fraction of $D^{*\pm}$ meson photoproduction due to diffractive exchange is consistent with the measurements of $D^{*\pm}$ meson production in diffractive deep inelastic scattering. Within the experimental uncertainties, this fraction shows no dependence on Q^2 and W .

The results demonstrate that diffractive open-charm photoproduction is well described by the dPDF parameterisations extracted from diffractive DIS data, supporting the validity of diffractive QCD factorisation. However, given the large experimental and theoretical uncertainties and the small hadron-like contribution expected by the NLO calculations, a suppression of the hadron-like component cannot be excluded.

9 Acknowledgments

We are grateful to the DESY Directorate for their strong support and encouragement. The effort of the HERA machine group is gratefully acknowledged. We thank the DESY computing and network services for their support. The design, construction and installation of the ZEUS detector have been made possible by the efforts of many people not listed as authors. It is a pleasure to thank H. Jung for useful discussions.

References

- [1] P.D.B. Collins, *An Introduction to Regge Theory and High-Energy Physics*, Cambridge University Press, Cambridge, 1977;
A.C. Irving and R.P. Worden, Phys. Rept. **34**, 117 (1977);
A.B. Kaidalov, *Regge Poles in QCD*, “At the Frontier of Particle Physics: Handbook of QCD“, M. Shifman (ed.), World Scientific (2002) (also preprint hep-ph/0103011).
- [2] L. Trentadue and G. Veneziano, Phys. Lett. **B 323**, 201 (1994).
- [3] A. Berera and D.E. Soper, Phys. Rev. **D 53**, 6162 (1996).
- [4] J.C. Collins, Phys. Rev. **D 57**, 3051 (1998); Erratum, ibid., **D 61**, 019902 (2000).
- [5] M.G. Ryskin, Sov. J. Nucl. Phys. **52**, 529 (1990);
E. Levin and M. Wusthoff, Phys. Rev. **D 50**, 4306 (1994);
A.D. Martin, M.G. Ryskin and G. Watt, Eur. Phys. J. **C 37**, 285 (2004);
A.D. Martin, M.G. Ryskin and G. Watt, Eur. Phys. J. **C 44**, 69 (2005);
G. Watt, *Proc. of the workshop "New Trends in HERA Physics 2005"*, Ringberg 2005, G. Grindhammer et al. (eds.), DESY conference proceedings (2005), p.303 (also preprint hep-ph/0511333).
- [6] H1 Collaboration, A. Aktas et al., Eur. Phys. J. **C 48**, 71 (2006).
- [7] ZEUS Collaboration, S. Chekanov et al., Eur. Phys. J. **C 38**, 43 (2004).
- [8] M. Groys, A. Levy and A. Proskuryakov, *Proc. of the workshop "HERA and the LHC"*, DESY-CERN 2004-2005, H. Jung and A. De Roeck (eds.), CERN-2005-014, DESY-PROC-2005-001 (2005), (also preprint hep-ph/0601012).
- [9] A.D. Martin, M.G. Ryskin and G. Watt, Phys. Lett. **B 644**, 131 (2007).
- [10] See e.g. V. Barone and E. Predazzi, *High-Energy Particle Diffraction*, Springer Verlag, Heidelberg, 2002, and references therein.
- [11] D. Graudenz and G. Veneziano, Phys. Lett. **B 365**, 302 (1996);
L. Alvero, et al., Phys. Rev. **D 59**, 074022 (1999);
C. Royon, Acta Phys. Polon. **B 37**, 3571 (2006).
- [12] G. Ingelman and P.E. Schlein, Phys. Lett. **B 152**, 256 (1985);
A. Donnachie and P. Landshoff, Phys. Lett. **B 191**, 309 (1987);
Erratum, ibid., **D 198**, 590 (1987).
- [13] A.B. Kaidalov et al., Eur. Phys. J. **C 21**, 521 (2001);
A.B. Kaidalov et al., Phys. Lett. **B 567**, 61 (2003).
- [14] CDF Collaboration, T. Affolder et al., Phys. Rev. Lett. **84**, 5043 (2000).

- [15] H1 Collaboration, C. Adloff et al., Phys. Lett. **B 520**, 191 (2001).
- [16] H1 Collaboration, A. Aktas et al., preprint DESY 06-164, preprint hep-ex/0610076, accepted by Eur. Phys. J. **C**.
- [17] ZEUS Collaboration, S. Chekanov et al., Phys. Lett. **B 545**, 244 (2002).
- [18] ZEUS Collaboration, S. Chekanov et al., Nucl. Phys. **B 672**, 3 (2003).
- [19] ZEUS Collaboration, U. Holm (ed.), *The ZEUS Detector Status Report* (unpublished), DESY (1993), available on <http://www-zeus.desy.de/bluebook/bluebook.html>.
- [20] N. Harnew et al., Nucl. Inst. Meth. **A 279**, 290 (1989);
B. Foster et al., Nucl. Phys. Proc. Suppl. **B 32**, 181 (1993);
B. Foster et al., Nucl. Inst. Meth. **A 338**, 254 (1994).
- [21] M. Derrick et al., Nucl. Inst. Meth. **A 309**, 77 (1991);
A. Andresen et al., Nucl. Inst. Meth. **A 309**, 101 (1991);
A. Caldwell et al., Nucl. Inst. Meth. **A 321**, 356 (1992);
A. Bernstein et al., Nucl. Inst. Meth. **A 336**, 23 (1993).
- [22] A. Bamberger et al., Nucl. Inst. Meth. **A 450**, 235 (2000).
- [23] ZEUS Collaboration, M. Derrick et al., Z. Phys. **C 63**, 391 (1994);
J. Andruszkow et al., Acta Phys. Pol. **B 32**, 2025 (2001).
- [24] ZEUS Collaboration, J. Breitweg et al., Eur. Phys. J. **C 1**, 81 (1998);
ZEUS Collaboration, J. Breitweg et al., Eur. Phys. J. **C 6**, 43 (1999);
G. Briskin, PhD Thesis, Tel Aviv University, Israel,
DESY-THESIS-1998-036, 1998.
- [25] A. Blondel and F. Jacquet, *Proc. of the workshop “Study of an ep Facility for Europe”*, ECFA, U. Amaldi (ed.), Hamburg, Germany, 1979, DESY 79-48, 391 (1979).
- [26] H. Jung, Comp. Phys. Comm. **86**, 147 (1995).
- [27] E. Berger et al., Nucl. Phys. **B 286**, 704 (1987);
K. Streng, *Proc. of the workshop “Physics at HERA”*, p. 365, R. Peccei (ed.), Hamburg, 1987, CERN-TH 4949 (1998).
- [28] H1 Collaboration, C. Adloff et al., Z. Phys. **C 76**, 613 (1997).
- [29] M. Glück, E. Reya, and A. Vogt, Phys. Rev. **D 51**, 3220 (1995).
- [30] V.N. Gribov and L.N. Lipatov, Sov. J. Nucl. Phys. **15**, 438 (1972);
V.N. Gribov and L.N. Lipatov, Sov. J. Nucl. Phys. **15**, 675 (1972);
L.N. Lipatov, Sov. J. Nucl. Phys. **20**, 94 (1975);

G. Altarelli and G. Parisi, Nucl. Phys. **B 126**, 298 (1977);
 Yu.L. Dokshitzer, Sov. Phys. JETP **46**, 641 (1977).

- [31] T. Sjostrand, Comp. Phys. Comm. **82**, 74 (1994);
 T. Sjostrand et al., Comp. Phys. Comm. **135**, 238 (2001).
- [32] G. Marchesini et al., Comp. Phys. Comm. **67**, 465 (1992);
 G. Corcella et al., JHEP **0101**, 010 (2001).
- [33] CTEQ Collaboration, H.L. Lai et al., Eur. Phys. J. **C 12**, 375 (2000).
- [34] B.R. Webber, Nucl. Phys. **B 238**, 492 (1984).
- [35] R. Brun et al., preprint CERN-DD/EE/84-1, CERN, 1987.
- [36] W.H. Smith, K. Tokushuku and L. W. Wiggers, *Proc. of int. conference “Computing in High-Energy Physics” (CHEP’92)*, Annecy, France, Sept. 1992, C. Verkerk and W. Wojcik (eds.), p. 222, CERN, Geneva, Switzerland (1992). Also in DESY 92-150.
- [37] S. Frixione et al., Nucl. Phys. **B 412**, 225 (1994).
- [38] S. Frixione et al., Nucl. Phys. **B 454**, 3 (1995);
 S. Frixione et al., Phys. Lett. **B 348**, 633 (1995);
 P. Nason, S. Dawson and R.K. Ellis, Nucl. Phys. **B 303**, 607 (1988).
- [39] S. Frixione et al., Phys. Lett. **B 319**, 339 (1993);
 C.F. von Weizsäcker, Z. Phys. **88**, 612 (1934);
 E.J. Williams, Phys. Rev. **45**, 729 (1934).
- [40] W.M. Yao et al. (Particle Data Group), J. Phys. **G 33**, 1 (2006).
- [41] L.K. Gladilin, preprint hep-ex/9912064, 1999;
 ZEUS Collaboration, S. Chekanov et al., Eur. Phys. J. **C 44**, 351 (2005).
- [42] C. Peterson et al., Phys. Rev. **D 27**, 105 (1983).
- [43] P. Nason and C. Oleari, Phys. Lett. **B 447**, 327 (1999).
- [44] ARGUS Collaboration, H. Albrecht et al., Z. Phys. **C 52**, 353 (1991).
- [45] P. Aurenche, J.P. Guillet and M. Fontannaz, Z. Phys. **C 64**, 621 (1994).
- [46] M. Glück, E. Reya, and A. Vogt, Phys. Rev. **D 46**, 1973 (1992).
- [47] ZEUS Collaboration, M. Derrick et al., Phys. Lett. **B 322**, 287 (1994).
- [48] ZEUS Collaboration, M. Derrick et al., Phys. Lett. **B 349**, 225 (1995);
 ZEUS Collaboration, J. Breitweg et al., Phys. Lett. **B 407**, 402 (1997);
 ZEUS Collaboration, J. Breitweg et al., Eur. Phys. J. **C 6**, 67 (1999);
 ZEUS Collaboration, J. Breitweg et al., Eur. Phys. J. **C 12**, 35 (2000).

- [49] ZEUS Collaboration, J. Breitweg et al., Phys. Lett. **B 401**, 192 (1997).
- [50] D. Bailey and R. Hall-Wilton, Nucl. Instr. and Meth. **A 515**, 37 (2003).
- [51] ZEUS Collaboration, S. Chekanov et al., Eur. Phys. J. **C 38**, 29 (2004).
- [52] ZEUS Collaboration, M. Derrick et al., Phys. Lett. **B 315**, 481 (1993);
ZEUS Collaboration, M. Derrick et al., Phys. Lett. **B 332**, 228 (1994).
- [53] ZEUS Collaboration, J. Breitweg et al., Eur. Phys. J. **C 6**, 67 (1999).

x_{P}	$d\sigma/dx_{\text{P}}$ (nb)
0.0 \div 0.004	51 \pm 11 $^{+ 6}_{- 5}$
0.004 \div 0.007	77 \pm 14 $^{+ 5}_{- 6}$
0.007 \div 0.010	63 \pm 12 $^{+ 5}_{- 6}$
0.010 \div 0.015	47.7 \pm 6.5 $^{+ 4.3}_{- 5.5}$
0.015 \div 0.020	39.6 \pm 8.7 $^{+ 5.8}_{- 5.5}$
0.020 \div 0.025	26.7 \pm 8.5 $^{+ 2.6}_{- 10.8}$
0.025 \div 0.035	27.0 \pm 6.3 $^{+ 4.7}_{- 4.7}$

Table 1: Differential cross section for diffractive photoproduction of D^* mesons as a function of x_{P} . The first column shows the bin ranges. The first and the second uncertainties are respectively statistical and systematic. The overall normalisation uncertainties due to the luminosity measurement (2.2%), the D^* and D^0 branching ratios (2%) and the proton-dissociative contribution subtraction (4.8%) are not indicated.

M_X (GeV)	$d\sigma/dM_X$ (pb/ GeV)	
	$x_{\text{P}} < 0.010$	$x_{\text{P}} < 0.035$
6 \div 13	$31.5 \pm 5.7^{+ 3.8}_{- 4.1}$	$31.9 \pm 5.8^{+ 3.8}_{- 4.1}$
13 \div 20	$42.9 \pm 7.4^{+ 2.5}_{- 3.8}$	$62.3 \pm 8.8^{+ 3.8}_{- 5.6}$
20 \div 27	$13.4 \pm 2.9^{+ 1.3}_{- 1.8}$	$57.5 \pm 7.5^{+ 6.6}_{- 7.0}$
27 \div 34	$0.04 \pm 0.74^{+0.004}_{-0.006}$	$36.2 \pm 7.4^{+ 4.5}_{- 6.2}$
34 \div 42	—	$12.2 \pm 3.6^{+ 1.4}_{- 2.6}$
42 \div 52	—	$5.6 \pm 2.8^{+ 2.4}_{- 1.1}$

Table 2: Differential cross sections for diffractive photoproduction of D^* mesons as a function of M_X for the two ranges $x_{\text{P}} < 0.035$ and $x_{\text{P}} < 0.01$. The first column shows the bin ranges. The first and second uncertainties are respectively statistical and systematic. The overall normalisation uncertainties due to the luminosity measurement (2.2%), the D^* and D^0 branching ratios (2%) and the proton-dissociative contribution subtraction (4.8%) are not indicated.

$p_T(D^*)$	$d\sigma/dp_T(D^*)$ (pb/ GeV)		$\mathcal{R}_D(p_T(D^*))$
(GeV)	$x_P < 0.010$	$x_P < 0.035$	(%)
1.9 \div 2.5	$443 \pm 105^{+37}_{-60}$	$1100 \pm 194^{+171}_{-145}$	$6.4 \pm 1.2^{+1.0}_{-0.9}$
2.5 \div 3.25	$308 \pm 63^{+23}_{-45}$	$596 \pm 85^{+52}_{-84}$	$6.1 \pm 0.9^{+0.5}_{-0.9}$
3.25 \div 4.0	$149 \pm 29^{+8}_{-19}$	$304 \pm 42^{+34}_{-39}$	$6.0 \pm 0.8^{+0.6}_{-0.8}$
4.0 \div 5.0	$18.3 \pm 4.9^{+1.2}_{-1.8}$	$85.8 \pm 13.1^{+7.2}_{-11.0}$	$3.5 \pm 0.5^{+0.3}_{-0.4}$
5.0 \div 6.0	$9.6 \pm 3.4^{+0.4}_{-1.0}$	$28.6 \pm 6.7^{+2.1}_{-3.0}$	$2.6 \pm 0.6^{+0.2}_{-0.3}$
6.0 \div 10.0	$0.35 \pm 0.35^{+0.03}_{-0.04}$	$5.09 \pm 1.2^{+1.0}_{-0.8}$	$2.0 \pm 0.5^{+0.4}_{-0.3}$
$\eta(D^*)$	$d\sigma/d\eta(D^*)$ (pb)		$\mathcal{R}_D(\eta(D^*))$
	$x_P < 0.010$	$x_P < 0.035$	(%)
-1.6 \div -1.2	$547 \pm 98^{+66}_{-79}$	$904 \pm 162^{+125}_{-125}$	$9.5 \pm 1.8^{+0.6}_{-1.2}$
-1.2 \div -0.8	$250 \pm 96^{+25}_{-35}$	$614 \pm 129^{+48}_{-78}$	$5.6 \pm 1.2^{+0.3}_{-0.7}$
-0.8 \div -0.4	$287 \pm 68^{+21}_{-39}$	$775 \pm 124^{+56}_{-90}$	$7.1 \pm 1.1^{+0.5}_{-0.8}$
-0.4 \div 0.0	$203 \pm 71^{+10}_{-24}$	$518 \pm 100^{+18}_{-51}$	$5.8 \pm 1.1^{+0.2}_{-0.6}$
0.0 \div 0.4	$158 \pm 45^{+7.3}_{-18}$	$394 \pm 78^{+49}_{-40}$	$5.0 \pm 1.0^{+0.6}_{-0.5}$
0.4 \div 0.8	$95 \pm 27^{+8.3}_{-11.8}$	$191 \pm 54^{+20}_{-32}$	$2.8 \pm 0.8^{+0.3}_{-0.5}$
0.8 \div 1.2	$55 \pm 30^{+4.7}_{-8.4}$	$220 \pm 69^{+36}_{-40}$	$4.0 \pm 1.3^{+0.7}_{-0.8}$
1.2 \div 1.6	$24 \pm 24^{+8.6}_{-8.9}$	$213 \pm 65^{+43}_{-55}$	$4.6 \pm 1.6^{+0.7}_{-1.1}$
$z(D^*)$	$d\sigma/dz(D^*)$ (pb)		$\mathcal{R}_D(z(D^*))$
	$x_P < 0.010$	$x_P < 0.035$	(%)
0.0 \div 0.2	$1080 \pm 191^{+74}_{-79}$	$2726 \pm 328^{+279}_{-166}$	$5.1 \pm 0.6^{+0.5}_{-0.4}$
0.2 \div 0.4	$960 \pm 315^{+152}_{-137}$	$2438 \pm 470^{+384}_{-207}$	$5.7 \pm 1.1^{+1.0}_{-0.6}$
0.4 \div 0.6	$735 \pm 121^{+67}_{-59}$	$1717 \pm 190^{+160}_{-107}$	$6.8 \pm 0.8^{+0.5}_{-0.4}$
0.6 \div 1.0	$157 \pm 46^{+45}_{-36}$	$234 \pm 74^{+55}_{-43}$	$5.3 \pm 1.7^{+1.1}_{-0.9}$

Table 3: Differential cross sections for diffractive photoproduction of D^* mesons for the two ranges $x_P < 0.035$ and $x_P < 0.01$ and diffractive fraction \mathcal{R}_D of D^* meson photoproduction as functions of $p_T(D^*)$, $\eta(D^*)$ and $z(D^*)$. The first column shows the bin ranges. The first and second uncertainties are respectively statistical and systematic. The overall normalisation uncertainties due to the luminosity measurement (2.2%), the D^* and D^0 branching ratios (2%) and the proton-dissociative contribution subtraction (4.8%) are not indicated.

W (GeV)	$d\sigma/dW$ (pb/ GeV)		$\mathcal{R}_D(W)$ (%)
	$x_P < 0.010$	$x_P < 0.035$	
130 \div 160	$2.7 \pm 1.3^{+0.5}_{-0.5}$	$8.8 \pm 1.9^{+0.7}_{-1.2}$	$3.9 \pm 0.9^{+0.3}_{-0.5}$
160 \div 190	$4.3 \pm 0.9^{+0.3}_{-0.6}$	$12.1 \pm 1.8^{+1.3}_{-1.4}$	$5.6 \pm 0.9^{+0.6}_{-0.7}$
190 \div 225	$4.5 \pm 1.2^{+0.3}_{-0.5}$	$10.6 \pm 1.7^{+1.1}_{-1.2}$	$6.3 \pm 1.1^{+0.6}_{-0.7}$
225 \div 265	$3.2 \pm 0.7^{+0.2}_{-0.4}$	$5.9 \pm 1.0^{+0.5}_{-0.7}$	$5.9 \pm 1.1^{+0.4}_{-0.7}$
265 \div 300	$3.2 \pm 0.7^{+0.2}_{-0.8}$	$6.1 \pm 1.1^{+0.5}_{-0.9}$	$6.7 \pm 1.2^{+0.4}_{-1.0}$

Table 4: Differential cross section for diffractive photoproduction of D^* mesons for the two ranges $x_P < 0.035$ and $x_P < 0.01$ and diffractive fraction \mathcal{R}_D of D^* meson photoproduction as a function of W . The first column shows the bin ranges. The first and second uncertainties are respectively statistical and systematic. The overall normalisation uncertainties due to the luminosity measurement (2.2%), the D^* and D^0 branching ratios (2%) and the proton-dissociative contribution subtraction (4.8%) are not indicated.

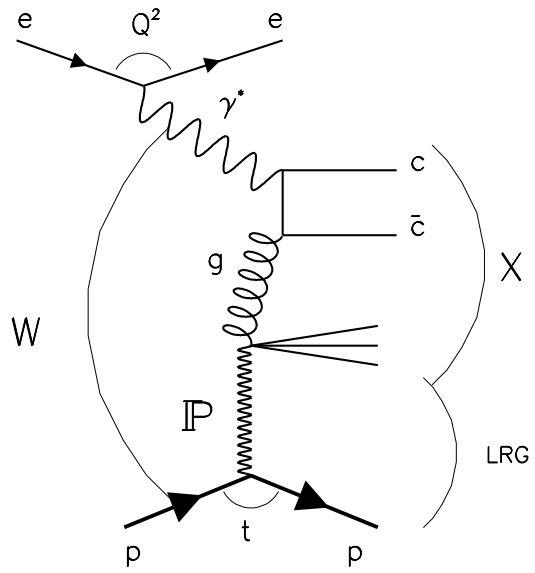


Figure 1: Example of charm production in diffractive ep scattering: boson-gluon fusion in the resolved-Pomeron model [12].

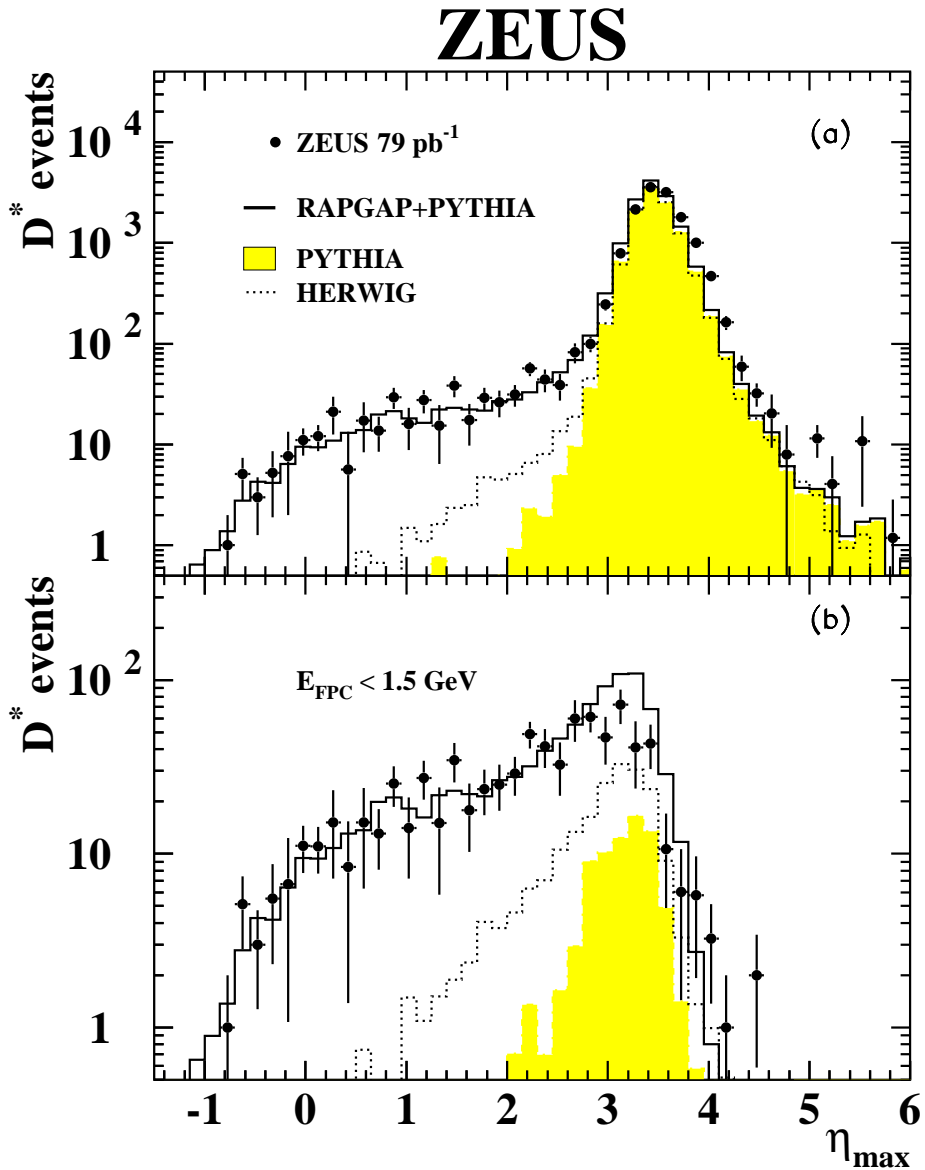


Figure 2: Comparison of the measured η_{max} distribution (dots) with the sum (solid histograms, normalised to the data) of the weighted diffractive (RAPGAP) and non-diffractive (PYTHIA, shaded histograms) MC distributions for (a) all inclusively photoproduced events with a reconstructed D^* meson and (b) events with $E_{FPC} < 1.5 \text{ GeV}$. The D^* mesons with $p_T(D^*) > 1.9 \text{ GeV}$ and $|\eta(D^*)| < 1.6$ were selected in the kinematic region $Q^2 < 1 \text{ GeV}^2$ and $130 < W < 300 \text{ GeV}$. The distributions for the non-diffractive events as predicted by HERWIG MC are indicated by the dotted histograms.

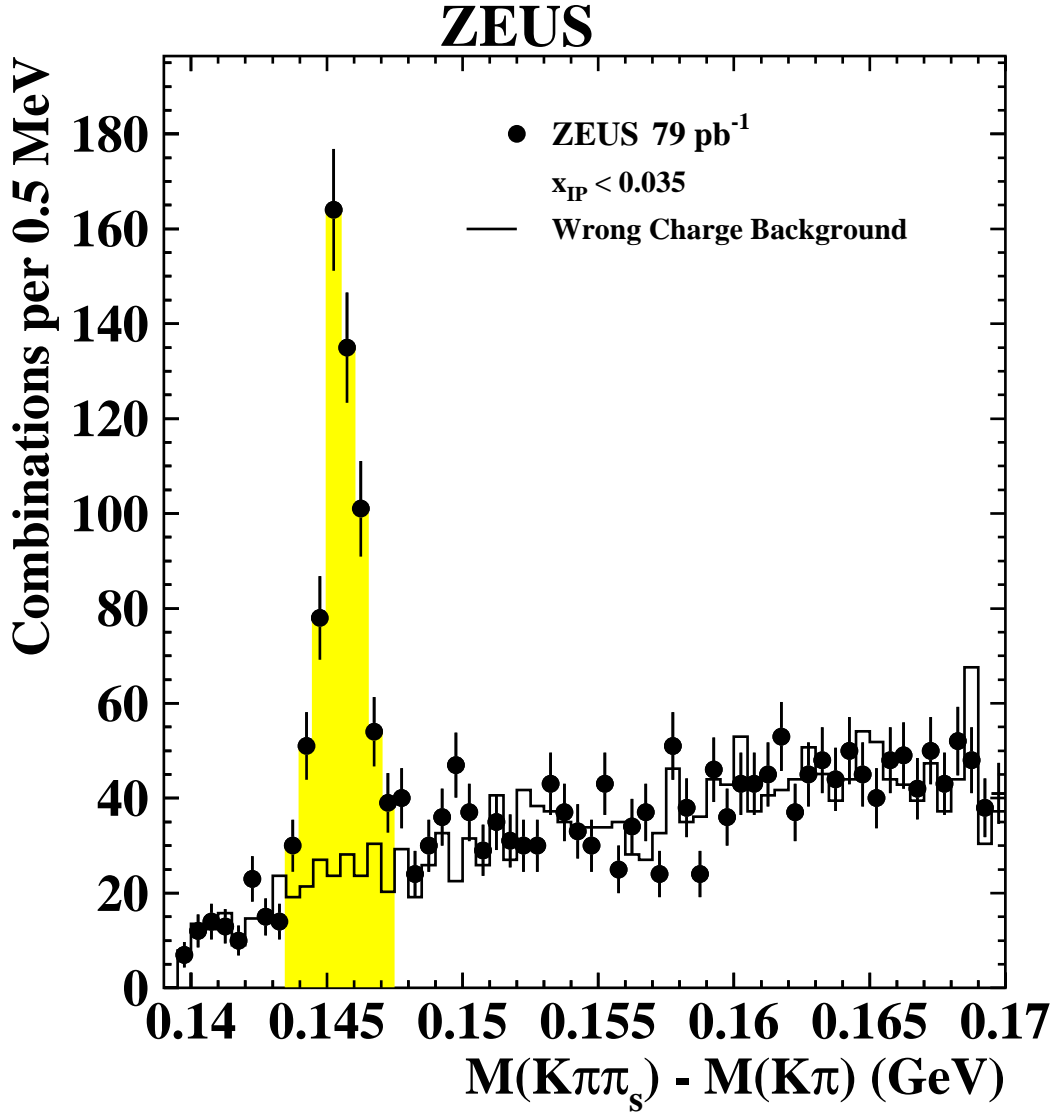


Figure 3: The distribution of the mass difference, $\Delta M = M(K\pi\pi_s) - M(K\pi)$, for the $D^*(2010)$ candidates (dots) with $p_T(D^*) > 1.9$ GeV and $|\eta(D^*)| < 1.6$, reconstructed for $Q^2 < 1$ GeV², $130 < W < 300$ GeV and $x_P < 0.035$. The shaded band shows the signal range, in which the combinatorial background (histogram) modelled by the wrong-charge combinations was subtracted. The signal contains 458 ± 30 D^* mesons.

ZEUS

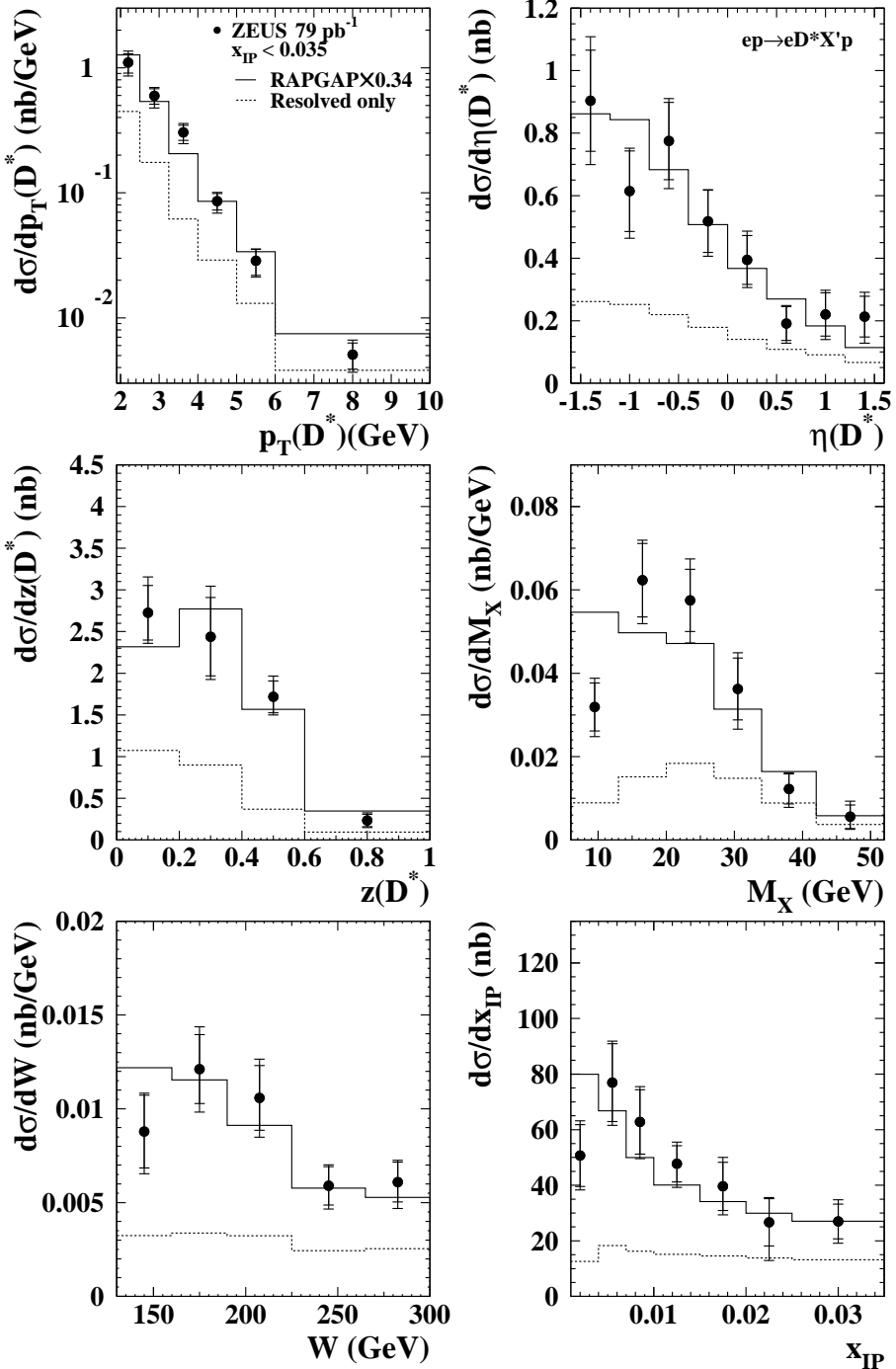


Figure 4: Differential cross sections (dots) for diffractive photoproduction of D^* mesons with respect to $p_T(D^*)$, $\eta(D^*)$, $z(D^*)$, M_X , W and x_{IP} measured for $x_{IP} < 0.035$. The inner bars show the statistical errors; the outer bars correspond to the statistical and systematic uncertainties added in quadrature. The data are compared to the prediction of RAPGAP (solid histograms) using the H1Fit2 LO diffractive parton distribution parameterisation. The theoretical prediction was normalised to the data. The dashed histograms show the predicted contribution from resolved photon processes.

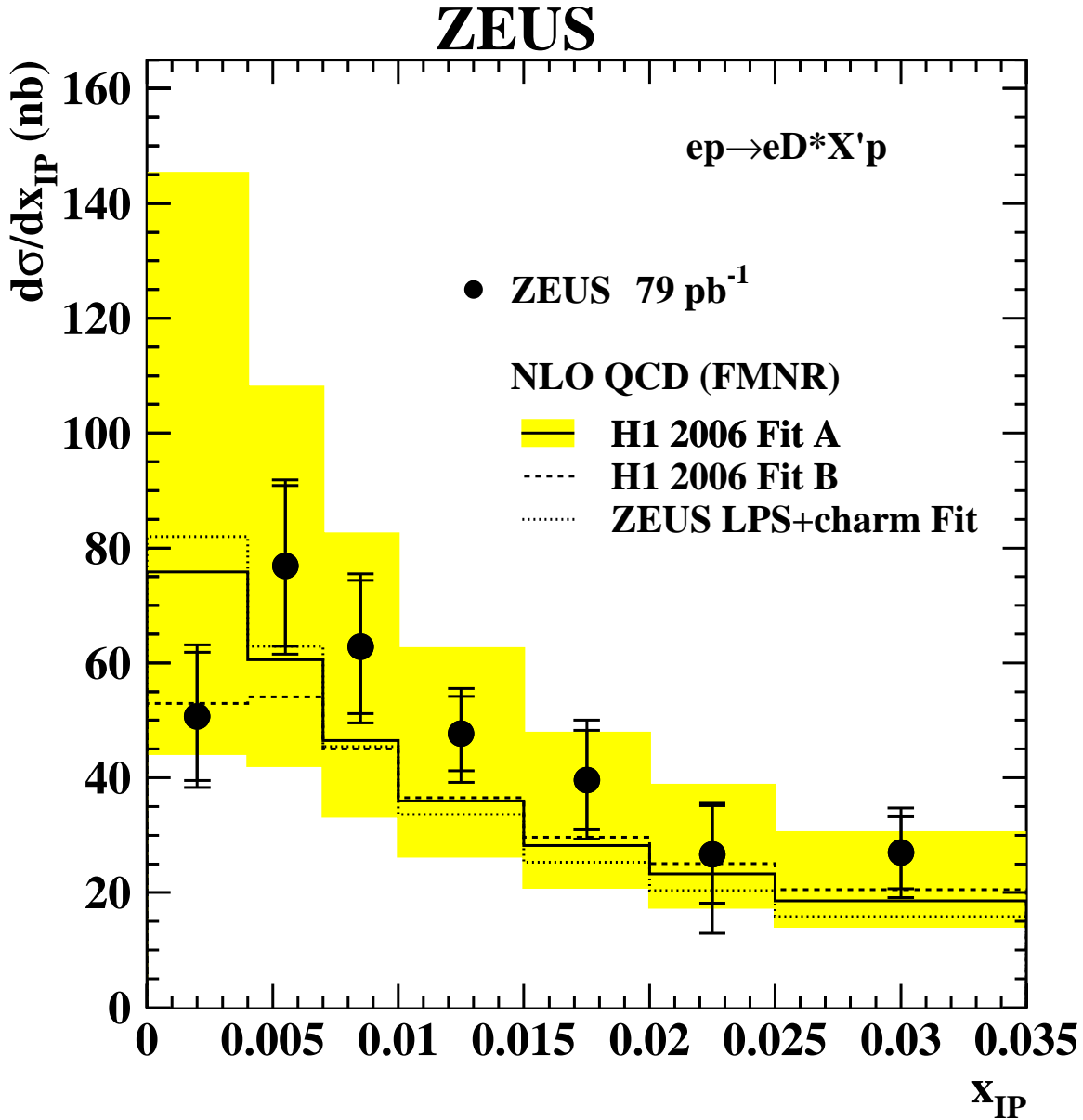


Figure 5: Differential cross section (dots) for diffractive photoproduction of D^* mesons, measured with respect to x_{IP} . The inner bars show the statistical errors; the outer bars correspond to the statistical and systematic uncertainties added in quadrature. The data are compared to the NLO QCD calculations (histograms) using the H1 2006 Fit A (solid), Fit B (dashed), both multiplied by a factor of 0.81, and the ZEUS LPS+charm Fit (dotted) diffractive parton distribution parameterisations. The shaded bands show the uncertainties coming from variations of the charm-quark mass and the factorisation and renormalisation scales.

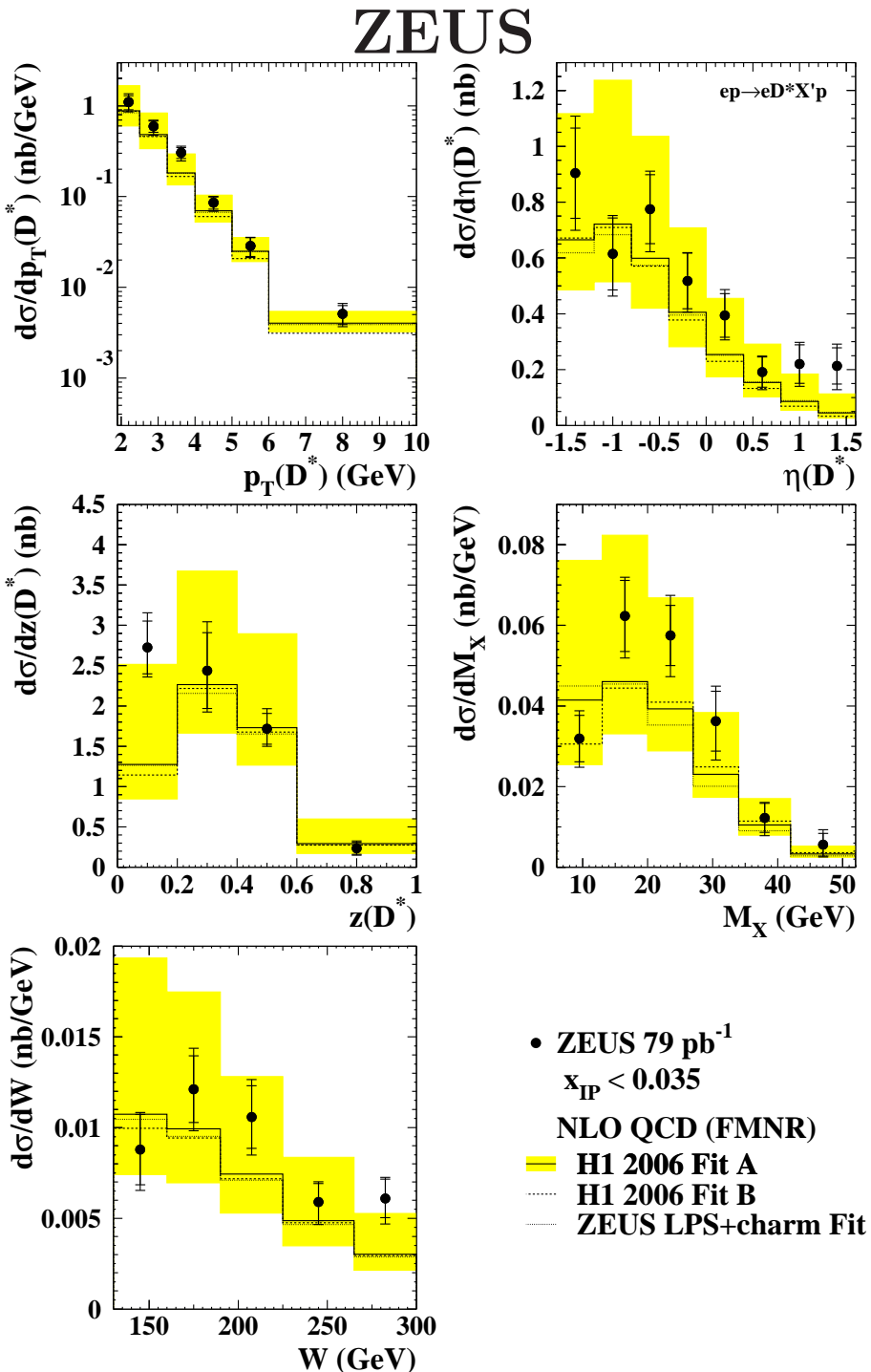


Figure 6: Differential cross sections (dots) for diffractive photoproduction of D^* mesons with respect to $p_T(D^*)$, $\eta(D^*)$, $z(D^*)$, M_X and W , measured for $x_{IP} < 0.035$. The inner bars show the statistical errors; the outer bars correspond to the statistical and systematic uncertainties added in quadrature. The data are compared to the NLO QCD calculations (histograms) using the H1 2006 Fit A (solid), Fit B (dashed), both multiplied by a factor of 0.81, and the ZEUS LPS+charm Fit (dotted) diffractive parton distribution parameterisations. The shaded bands show the uncertainties arising from variations of the charm-quark mass and the factorisation and renormalisation scales.

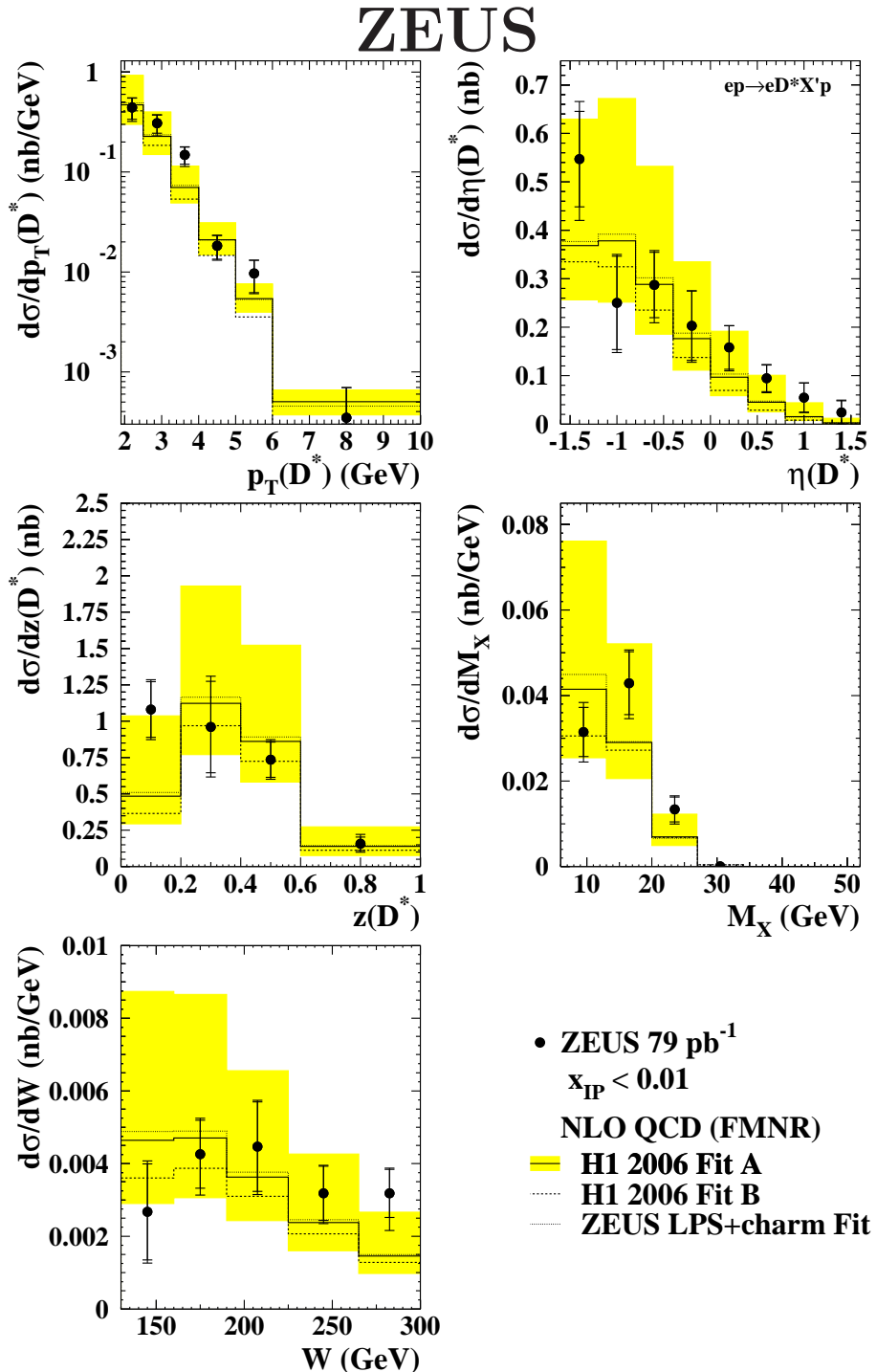


Figure 7: Differential cross sections (dots) for diffractive photoproduction of D^* mesons with respect to $p_T(D^*)$, $\eta(D^*)$, $z(D^*)$, M_X and W , measured for $x_{IP} < 0.01$. The inner bars show the statistical errors; the outer bars correspond to the statistical and systematic uncertainties added in quadrature. The data are compared to the NLO QCD calculations (histograms) using the H1 2006 Fit A (solid), Fit B (dashed), both multiplied by a factor of 0.81, and the ZEUS LPS+charm Fit (dotted) diffractive parton distribution parameterisations. The shaded bands show the uncertainties arising from variations of the charm-quark mass and the factorisation and renormalisation scales.

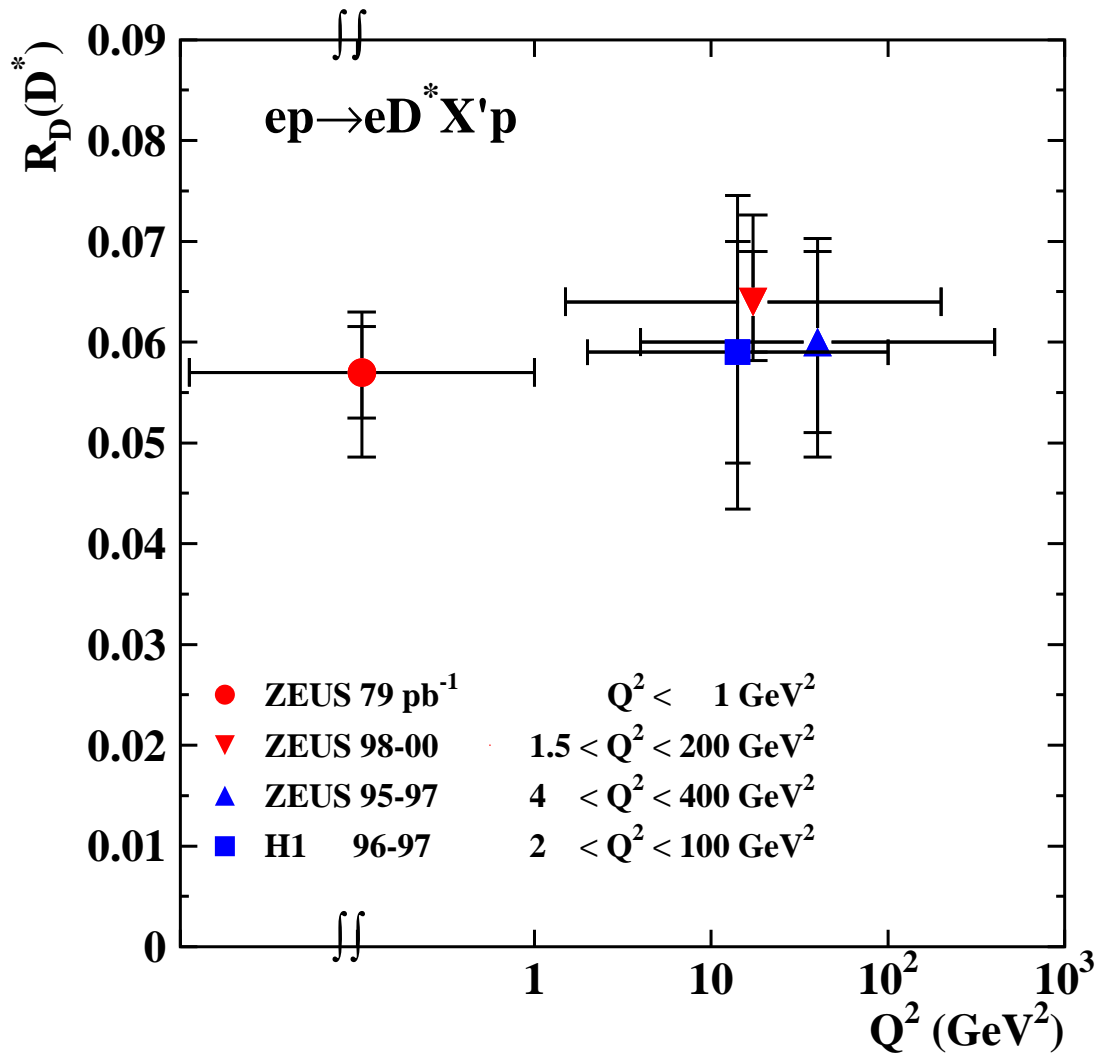


Figure 8: Fractions R_D of D^* meson diffractive production cross sections measured at HERA in DIS [15, 17, 18] and photoproduction (this measurement). The inner bars show the statistical errors, and the outer bars correspond to the statistical and systematic uncertainties added in quadrature.

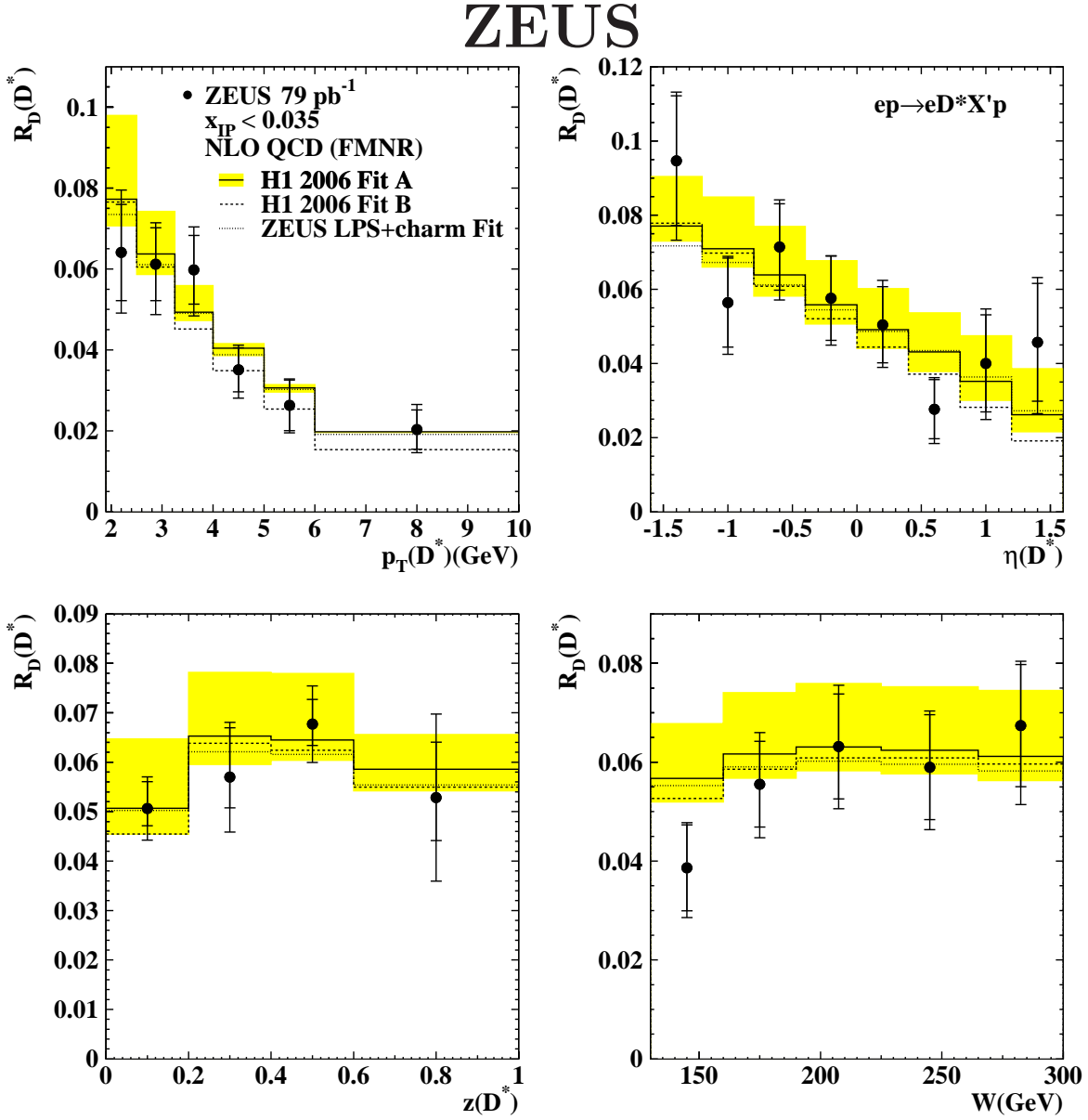


Figure 9: Fraction of D^* meson diffractive photoproduction as a function of $p_T(D^*)$, $\eta(D^*)$, $z(D^*)$ and W . The inner bars show the statistical errors; the outer bars correspond to the statistical and systematic uncertainties added in quadrature. The data are compared to the NLO QCD calculations (histograms) using the H1 2006 Fit A (solid), Fit B (dashed), both multiplied by a factor of 0.81, and the ZEUS LPS+charm Fit (dotted) diffractive parton distribution parameterisations. The shaded bands show uncertainties arising from variations of the charm-quark mass and the factorisation and renormalisation scales.